Numerical Investigation of the Properties of Unreinforced and Reinforced Nepalese Historical Brick Masonry Structures

Chhabi Mishra[1], Kentaro Yamaguchi[2(✉)], Tingyun Jing[1], Toshikazu Hanazato[3], Yohei Endo[4], and Manjip Shakya[5]

[1] Department of Architecture, Graduate School of Human-Environment Studies, Kyushu University, Fukuoka, Japan
chhabi.mishra7@gmail.com
[2] Department of Architecture and Urban Design, Faculty of Human-Environment Studies, Kyushu University, 744 Motooka , Nishi-u 819-0395, Fukuoka, Japan
yamaguchi@arch.kyushu-u.ac.jp
[3] Laboratory for Engineering, Kanagawa University, Yokohama, Japan
hanazato@arch.mie-u.ac.jp
[4] Department of Architecture, Faculty of Engineering, Shinshu University, Nagano, Japan
endii@shinshu-u.ac.jp
[5] Khwopa Engineering College, Purbanchal University, Bhaktapur, Nepal
maanzeep@gmail.com

Abstract. Considering the limited strength of traditional masonry structures, retrofitting is essential. The purpose of this study was to discretize a numerical model that can be used to assess the behavior of brick masonry in earth mortar. The behavior of unreinforced brick masonry (URM) and brick masonry reinforced with timber was investigated through numerical simulation. The flexural strength of URM and reinforced masonry prism of size 280 mm x 350 mm x 860 mm (B x D x L) was calculated by three-point bending experiments. For reinforced masonry prism, ladder and diagonal brace reinforcement with timber were studied. From the results, it was observed that the diagonal brace reinforced prism withstood higher flexural tensile stress compared to the URM and ladder reinforced prisms. From the uniaxial compression test conducted on the same size of masonry prism, the elastic modulus (E) calculated was 310 MPa. A homogenous macro model was used in ABAQUS software to reproduce a previously performed three-point bending test of a prism built of brick masonry in earth mortar. Material properties such as density, E, and Poisson's ratio were input to the software. The displacement value obtained was very low compared to the experimental result when E of 310 MPa determined from the uniaxial compression test was taken. The reason might be due to the involvement of both tensile and compressive forces in the bending test. In this study, the elastic modulus in tension (E_t) was considered 1/5 of that in compression (E_c) for URM prism. Numerical model for the URM prism gave closer results to experimental value when E_c was 41 MPa, which was 1/8 of E determined from the uniaxial compression test (310 MPa). In uniaxial compression test, the direction of compressive strut formed was 90° to the bed angle. However, in three-point bending test, a compressive strut was formed from

Y. Endo and T. Hanazato (Eds.): SAHC 2023, RILEM Bookseries 46, pp. 125–139, 2024.
https://doi.org/10.1007/978-3-031-39450-8_11

the point of loading to the supports. For URM and diagonal braced specimen compressive strut formed was 56.3° to the bed angle (θ_{strut}), whereas for ladder reinforced specimen, it was 37.2°. For the ladder and diagonal braced reinforced model, crack was assumed at the tensile side of the masonry. By trial and error, the numerical result was in good agreement with the experimental value for maximum displacement at the mid-point under the condition that the E of 20.5 MPa and 41.0 MPa was taken for the ladder and diagonal brace model, respectively, with a 70 mm crack at the tensile side of masonry. In the analysis, it was observed that for URM and diagonal brace reinforced model, E was greater than for the ladder reinforced model. Namely, with the increase in compressive strut angle (θ_{strut}), there was an increase in the value of E.

Keywords: Historical · Masonry · Numerical modeling · Retrofitting · Sal timber

1 Introduction

1.1 Masonry in Earth Mortar

Mechanical Behavior of Masonry in Earth Mortar. There are a large number of non-engineered constructions still exist in many parts of the world which are mostly constructed with locally available materials such as stones, bricks or adobe joined together with mortar [1]. About 30% of the world's population lives in earth building [2]. These buildings are constructed by local masons based on experience and knowledge and are vulnerable to earthquakes [3]. Earth construction is widely spread and the oldest type of construction. The historical buildings constructed with brick and mud mortar are vulnerable to earthquakes due to the low strength of materials, poor structural detailing, and lack of seismic design and thus require seismic protection [4]. Compressive strength, elastic modulus, and shear modulus are mechanical properties that are required to analyze and design masonry structures. The value of mechanical properties varies widely depending on the quality of materials, size, and workmanship of construction [5]. An experimental investigation is needed for understanding the mechanical behavior of earth building properly [2, 6].

Strengthening of Masonry in Earth Mortar. Retrofitting of unreinforced brick masonry (URM) buildings is important as they are vulnerable to damage against in-plane and out-of-plane failure due to limited shear strength, flexural strength, and deformation capacity [7]. Timber panels are used in masonry structures with earthen mortar to enhance the integrity of the masonry walls [8]. Moreira et al. [9] reported that ductility was increased by retrofitting the masonry wall with a timber frame in their quasi-static monotonic and cyclic pull-out tests. Sustersic and Dujic [10] reported that the strength and ductility of URM were increased by retrofitting with Cross Laminated Timber (CLT) panels. The plywood panels can withstand diagonal tension forces compared to timber frames [11]. Retrofitting with timber strong-back prevents the out-of-plane failure of masonry walls [12].

1.2 Numerical Analysis of Masonry in Earth Mortar

For the reliability and accuracy of the numerical model, the material properties are necessary based on experimental results. Once the model is calibrated, it is possible to vary the desired parameters and verify the effect of each component [13]. The modeling strategies can be classified as detailed micro-modeling, simplified micro-modeling, and macro-modeling [14]. In micro-modeling technique, the units, mortar, and the unit-mortar interface are modeled separately. However, in macro modeling, no distinction is made between units and joints, and masonry is modeled as a homogeneous material with equivalent material properties [15]. A macro model which is easy to use for structural design, seismic diagnosis, and retrofitting was used in this study. The purpose of this study was to discretize a numerical model that can be used to assess the behavior of brick masonry in earth mortar. The behavior of URM and brick masonry reinforced with timber was investigated through numerical simulation.

2 Materials and Methods

2.1 Description of the Experiment

Uniaxial compression experiments were conducted to clarify the basic mechanical properties of elements of brick walls (unit bricks, mud mortar, and masonry prisms) [16]. The bulk density of the masonry prism was 1566 kg/m^3, which was calculated from the proportion of brick and mud mortar in a prism. To study the flexural behavior of the wall, six prism specimens with dimensions of 280 mm × 350 mm × 860 mm (B × D × L) were constructed by brick and mortar, namely B5U1, B6U2, B1L1, B2L2, B3B1, and B4B2, respectively [6]. In the bending experiment, the B5U1 and B6U2 were unreinforced specimens (Fig. 1a), while the rest of the four specimens were reinforced with timber (Sal wood). The specimens (B1L1 and B2L2) were reinforced with ladder-type reinforcement (Fig. 1b), and the other two (B3B1 and B4B2) were reinforced with diagonal type braces (Fig. 1c). The cross-section of the timber plate was 50 × 10 mm^2 and was connected by steel bolts of 12 mm diameter.

The load of 100 kN was applied manually by a mechanical jack. The jig system and displacement transducers were also used. Three-point bending tests were carried out on prisms that were set vertically and horizontal force was applied at the center of the prism. Supports were fixed at the top and bottom of the prisms. Displacement transducers were set up at the top, middle, and bottom of the prisms.

Calculation of Flexural Strength and Deformation Angle. The flexural strength fr was calculated using Eq. (1),

$$Fr = \frac{(1.5Pl)}{(BD^2)} \tag{1}$$

where,

P is the maximum load taken by the specimen,
Fr is the flexural strength of the masonry prism,
l is the support span of the member;

B is the width of the specimen and
D is the thickness of the specimen.

To estimate the net displacement in the specimen mid-height, the average value of horizontal displacement at the top and bottom of the specimen was removed from the mean value of the displacement measured at the specimen mid-height. From the displacement measured, the deformation angle was calculated.

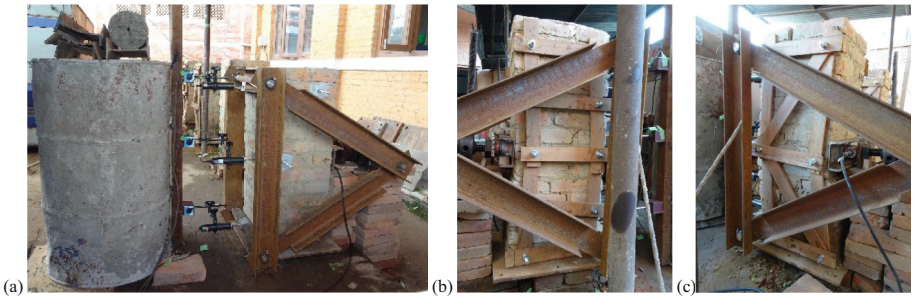

Fig. 1. Bending test setup (a) URM specimen (b) ladder reinforced specimen and (c) diagonal brace reinforced specimen

2.2 Research Methodology

The present research was composed of the following three stages. First, a case study on the results obtained in bending experiments of brick masonry that constitutes historical buildings in Nepal is presented. The three-point loading test on the URM prism and reinforced masonry prism with wood (SAL timber) and bolts was performed. Second, for numerical modeling, elastic regions were determined from a graph of flexural stress-deformation angle. The first crack point was identified from experimental data and was also confirmed by basic mechanics theories. Third, numerical analysis was performed on the bending test models. This stage was articulated in two steps, which included (i) validation of the URM prism, and (ii) validation of the retrofitted masonry prism with timber panels. The numerical models were developed and validated using a macro model elastic analysis. The general-purpose finite element method software ABAQUS was used for the analysis. As the micro model is complicated to be used for historical buildings and requires longer time and effort, this research aims to develop an analysis method that can more easily reflect the behavior of actual structures by using macro modeling. In addition, it is not realistic to design structures that cause large deformations in the case of brittle masonry; hence this study mainly focuses on small deformation regions that can be used for safer structural design.

The purpose of this study was to discretize a numerical model that can be used to assess the behavior of brick masonry in earth mortar. The behavior of URM and brick masonry reinforced with timber was investigated through numerical simulation. In general, for macro-modeling same elastic modulus (E) is assumed for compression and tension. In our study, the flexural modulus of elasticity (E_b) was 14.816 MPa which was

several times lower than E determined from the uniaxial compression test (310 MPa). When E of 310 MPa was used as input to the software, the displacement value obtained was very low compared to the experimental result. The reason might be due to the involvement of both tensile and compressive forces in the bending test. Kanno et al. [17] reported that for URM, E_c is 5–6 times higher than the (E_t). For URM, E_t was assumed as 1/5 of the E_c. By trial and error, the numerical result was matched with the experimental value for maximum displacement at the mid-point. For reinforced masonry, cracks were assumed at the tensile side of the masonry at about a depth of 70mm, 90 mm, and 130 mm. By trial and error, the numerical result was matched with the experimental value for maximum displacement at the mid-point for the crack introduced model. The calibrated value of E for the diagonal brace reinforced model was compared to the ladder reinforced model. The effect of compressive strut angle formed in the specimen was also studied.

2.3 Results and Discussion

Figure 2 shows the flexural stress versus deformation angle curve for all specimens. The values in the graph show the maximum flexural stress of each specimen. The flexural strength was increased in reinforced specimens.

Failure Modes of URM and Reinforced Prism Specimens. For URM, the specimen starts taking load and suddenly decreases when opening starts due to tensile splitting. However, due to the strut mechanism, the specimen again starts taking load. The flexural strength was increased in reinforced specimens showing the maximum for diagonal braced rein-forced prism, however sudden drop was observed in the graph when maximum load was reached which was also evidenced by the sudden split in the specimen, whereas the failure in ladder reinforced prism was mild and cracks were dispersed all over the specimen. Among ladder reinforced specimens, specimen B1L1 was damaged before loading and as a result, the graph was slightly different from specimen B2L2 which shows a smooth curve.

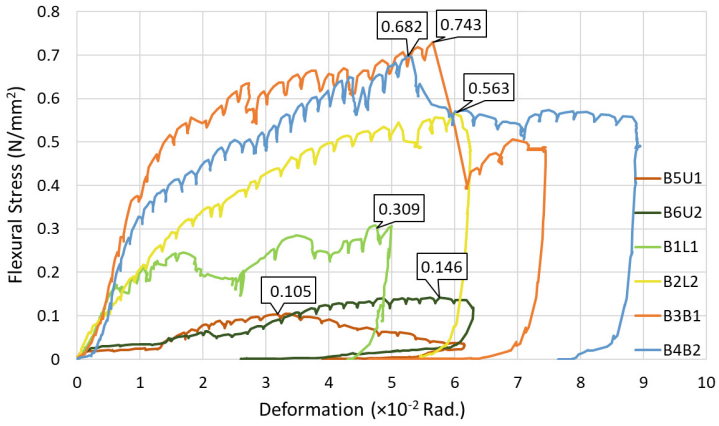

Fig. 2. Flexural stress versus deformation angle curve for all the specimens

Calculation of Restoring Force Characteristics. First, the elastic-plastic deformation range was determined. The elastic-plastic range and the deformation angle of each masonry prism for the bending experiment are shown in Table 1. First and second crack points A and B were determined as the intersections of linear regressions as shown in Fig. 3a. The flexural stress versus deformation angle curves of URM, ladder reinforced, and diagonal braced reinforced specimens are shown in Fig. 3b, 3c, and 3d, respectively. The flexural stress versus deformation angle curves for all specimens are shown in Fig. 3e.

Table 1. Deformation range of URM and reinforced specimens

Specimens	Elastic deformation ($\times 10^{-2}$ rad)	Plastic deformation ($\times 10^{-2}$ rad)
URM (B5U1, B6U2)	0–0.10	0.10–1.33
Ladder (B1L1, B2L2)	0–0.95	0.95–2.00
Brace (B3B1, B4B2)	0–0.75	0.75–2.00

Table 2. Calculation of first and second crack points, load, horizontal displacement, and flexural modulus at first crack points

Specimens	First crack point		Second crack point		Stiffness in elastic deformation (N/mm^2)	Stiffness in plastic deformation (N/mm^2)	Load P at first crack (N)	Horizontal displacement at first crack (mm)	Flexural modulus at first crack E_b (MPa)
	Deformation ($\times 10^{-2}$ rad)	Stress (N/mm^2)	Deformation ($\times 10^{-2}$ rad)	Stress (N/mm^2)					
URM	0.095	0.020	1.330	0.032	0.2103	0.0099	618	0.352	14.816
Ladder	0.954	0.211	2.000	0.294	0.2214	0.0788	6520	3.533	15.573
Brace	0.804	0.389	2.026	0.549	0.4839	0.1308	12020	2.978	34.061

The bilinear characteristics of restoring force for URM prism were calculated by the first crack point, the second crack point, the elastic deformation, and the plastic deformation. The first crack point was obtained from experimental data when the deformation increased rapidly compared to flexural stress. The elastic deformation is the range from the beginning of the experiment till the first crack point. The URM prism is elastic for a small deformation. The second crack point was obtained from the experimental data when the ratio of change in deformation was less compared to the increase in flexural stress. The plastic deformation was in the range from the first crack point to the second crack point. The characteristics of restoring force for URM and reinforced masonry specimens were determined as shown in Fig. 4. Deformation, the stress at the first crack point, the stiffness of elastic deformation range, and the stiffness of plastic deformation range are shown in Table 2. The stiffness of the elastic deformation of the ladder and diagonal brace reinforced specimens were 1.05 times and 2.30 times greater than the stiffness of the elastic deformation of URM specimens, respectively. However, the stiffness of the plastic deformation range of the ladder and diagonal brace reinforced specimens were 7.96 times and 13.21 times greater than the stiffness of the plastic deformation of the

URM specimen. Stiffness reduction from the elastic area to the plastic area of URM, ladder, and diagonal brace reinforced specimen were 0.0471 times, 0.356 times, and 0.270 times, respectively.

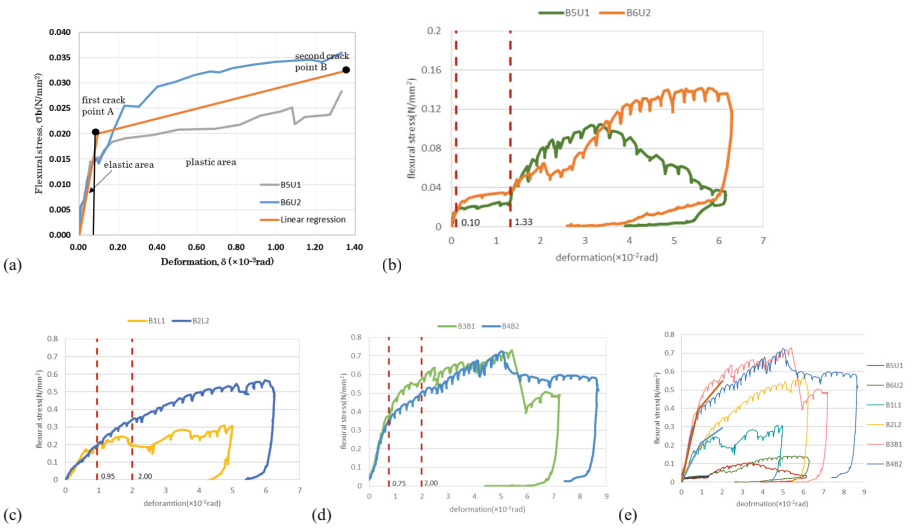

Fig. 3. Flexural stress versus deformation angle curves of specimens (a) Crack points and elastic-plastic deformations range of URM specimens (b) URM specimens (c) Ladder reinforced specimens (d) Diagonal brace reinforced specimens (e) All prism specimens

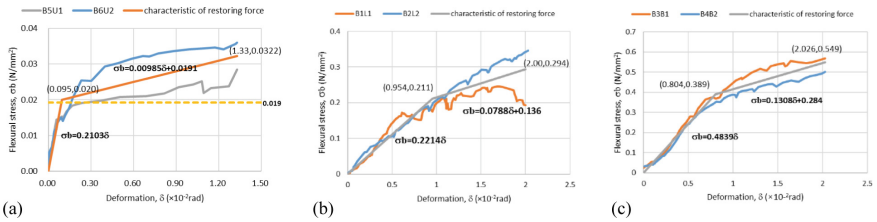

Fig. 4. Characteristics of restoring force for URM and reinforced specimens (a) URM specimen (b) Ladder reinforced specimen (c) Diagonal brace reinforced specimen

Load Calculation During Rigid Body Rotation of URM Specimens. The URM prism, subjected to the horizontal load applied from a hydraulic Jack is shown in Fig. 5a. The load was calculated from Eqs. (2) and (3) when the masonry prism began to rigid body rotation [18].

$$\sum M_B = Q \times \frac{L}{2} - W \times \frac{D}{2} \tag{2}$$

$$\sum F_x = P - Q - Q = 0 \tag{3}$$

where,

Q is the reaction force at the top and bottom supports,
W is the self-weight of half of the masonry prism,
P is the horizontal force from the hydraulic jack,
D is the depth of the masonry prism, and
L is the height of the masonry prism.

The calculated value of horizontal force (P) when rigid body rotation occurred was 609 N. At a stress of 0.019 N/mm^2, the URM specimen started rigid body rotation which was close to the stress in the first crack point of URM specimen (Fig. 4a). Figure 5b shows the load at rigid body rotation and load at the first crack point.

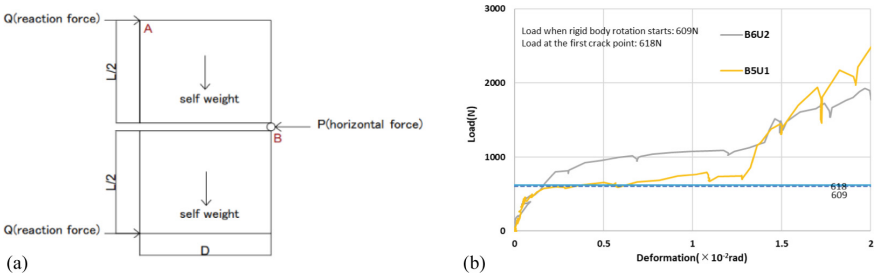

Fig. 5. (a) Horizontal and reaction force of bending experiment (b) Load at rigid body rotation and load at first crack point

Flexural Modulus for Bending Test. Flexural modulus (E_b) for Bending test specimens was determined as follows.

$$Eb = \frac{l^3}{4BD^3} \times \frac{\Delta P}{\Delta \delta} \tag{4}$$

where, D is the depth of the masonry prism, B is the width of the cross-section, l is the span of the masonry prism, $\Delta P/\Delta\delta$ is the ratio of the elastic range of load and deflection.

The load, deflection, and flexural modulus at the first crack point of all masonry prisms are shown in Table 2. Flexural modulus (E_b) of masonry prisms calculated from Eq. (4) was less than E determined from uniaxial compression experiment (310 MPa) due to anisotropic behavior of brick masonry with low strength mortar.

Determination of Poisson's Ratio. Figure 6a shows the shear stress versus tensile/compressive strain of the diagonal compression experiment for D2 and D6 Specimens. Poisson's ratio was calculated as the ratio of strain in the tensile direction to the compressive direction as the difference in tensile and compressive strain were large in the diagonal experiment (Fig. 6a). Tensile strain is the elongation in the tensile diagonal direction measured by displacement transducer L2 (Fig. 6b). Similarly, compressive strain is the shortening in the compressive diagonal direction measured by displacement transducer L1 (Fig. 6b). Poisson's ratio was calculated by taking linear regression of data up to 33% of maximum load (Fig. 6c). The Poisson's ratio of D2 and D6 specimens were 0.0705 and 0.0260, respectively. The average Poisson's ratio was 0.0483.

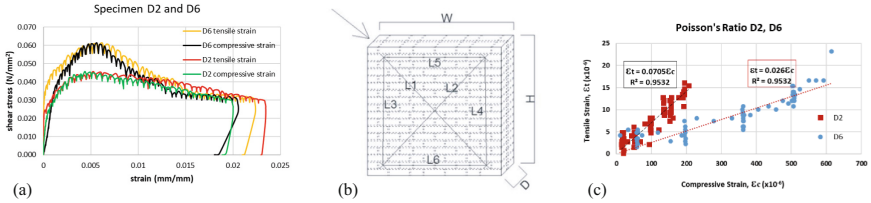

Fig. 6. Diagonal compression experiment (a) Shear stress versus compressive/tensile strain (b) Schematic diagram of specimen in diagonal compression experiment (c) Tensile strain versus compressive strain for D2 and D6 specimen

3 Numerical Modeling of URM and Reinforced Masonry Prisms

3.1 Numerical Modeling of Masonry Prism

A numerical model of a masonry prism was created using a three-dimensional solid (or continuum) element in ABAQUS finite element software. C3D8R is a hexahedral 8-node linear brick element with reduced integration (one integration point). The integration point of the C3D8R element is located in the middle of the element. C3D8R was selected for mesh generation as it is cost-effective and has enhanced convergence compared to full integration [14].

A mesh size of 30 mm was used. The size of URM, ladder reinforced, and diagonal brace reinforced model was 350 mm × 280 mm × 860 mm. Masonry was modeled as an isotropic and homogeneous material. The sizes of steel plates used at the top, bottom, and base supports were 280 mm × 20 mm × 100 mm, and a friction coefficient of 0.30 was taken for the interface between masonry and steel plates [14]. In ladder and diagonal brace models, brick masonry prisms were reinforced with timber of cross-section 50 mm × 10 mm. The timber reinforcement was connected to a brick masonry prism with 12 mm bolts by multi-point constraints (MPC). MPC is used to connect the elements between them and to impose constraints between different degrees of freedom of the model. The MPC is a rigid body between two nodes to constrain the displacement and rotation at the first node to the displacement and rotation at the second node. The bolt was considered a one-dimensional element and timber plate and brick masonry were considered as three-dimensional elements. There were three boundary conditions (BC), namely top BC, bottom BC, and base BC in the modeling to replicate the experimental condition (Fig. 7a). For URM, ladder reinforced and diagonal brace reinforced specimens load was applied in terms of pressure 0.02207 N/mm^2, 0.2329 N/mm^2 and, 0.2329 N/mm^2, respectively. The timber material properties were taken as input to the software (Table 3) [19]. Poisson's ratio and density were also taken as input to the software. Elastic modulus (E) from the prism compression experiment was taken as the E initial for the first iteration. The trials for different values of E during modeling were done until the numerical result was in good agreement with the experimental value for maximum displacement at the mid-point.

Table 3. Mechanical properties of masonry, steel, and timber

Materials	Elastic modulus E (MPa)	Poisson's ratio	Density (kg/mm^3)
Masonry	23	0.0483	1.57×10^{-6}
Steel	205000	0.30	7.85×10^{-6}
Timber (SAL)	20500	0.40	8.86×10^{-7}

3.2 Output of URM Model

The 3D model, tensile principal stress, and compressive principal stress contour for the URM model are shown in Fig. 7a-c, respectively. The stress contours show the part under load was in compression, and the part away from the load was in tension, which was in good agreement with the experimental result. The numerical result was in good agreement with the experimental value for maximum displacement (0.352 mm) at the mid-point when E (23 MPa) was taken (Table 4).

3.3 Output of Ladder Reinforced Model

The 3D model, tensile principal stress, and compressive principal stress contour for ladder reinforced model are shown in Fig. 8a-c respectively. The compressive strut in masonry is formed in the ladder reinforced model as shown in Fig. 8c. The numerical result was in good agreement with the experimental value for maximum displacement (3.533 mm) at the mid-point when E (16.45 MPa) was taken (Table 4).

3.4 Output of Diagonal Brace Reinforced Model

The 3D model, tensile principal stress, and compressive principal stress contour for the diagonal brace reinforced model are shown in Fig. 9a-c respectively. The numerical result was in good agreement with the experimental value for maximum displacement (1.615 mm) at the mid-point when E (38 MPa) was taken (Table 4).

In the ladder reinforced model, E (16.45 MPa) used for best fit was smaller compared to E (24 MPa) for the URM model and E (38 MPa) for the diagonal brace reinforced model.

3.5 Effect of Strut Angle on the Elastic Modulus for Reinforced Masonry Model

In a ladder type, the compressive/strut mechanism is formed due to a ladder-type truss, similar to a reinforced concrete beam. The compressive force in a diagonal direction is the compressive force of masonry, which is the shear resistance mechanism in a beam. Similarly, in the diagonal brace type, the tensile force in diagonal timber members is effective to resist the compressive force of masonry. Due to the formation of truss mechanism in the ladder reinforced model, the strut angle (θ_{strut}) of ladder reinforced model was smaller compared to the diagonal brace reinforced model. For URM and diagonal braced specimen compressive strut formed was 56.3° to the bed angle (θ_{strut}), whereas for ladder reinforced specimen, it was 37.2°. The ladder and diagonal brace reinforced specimens take higher loads even after the crack is developed in the masonry. Hence, the tensile cracks were assumed at the tensile side of masonry in reinforced specimens at about a depth of 70 mm, 90 mm, and 130 mm (Fig. 10b-c). The numerical and experimental results by assuming a crack in the tensile side of masonry of the reinforced model is shown in Table 5. In the ladder reinforced model, after the introduction of a crack of 70 mm, 90 mm, and 130 mm at the tensile side of the masonry, the numerical result was in good agreement with the experimental value for maximum displacement (3.533 mm) at the mid-point when E of 20.5 MPa, 22.5 MPa, and 27 MPa was taken, respectively. Similarly, in the diagonal brace reinforced model, after the introduction of a crack of 70mm, 90 mm, and 130 mm at the tensile side of the masonry, the numerical result was in good agreement with the experimental value for maximum displacement (1.615 mm) at the mid-point when E of 41 MPa, 43 MPa, and 47 MPa were taken, respectively. The numerical result matched the experimental value with an increased value of E for both the ladder and diagonal braced reinforced models compared to the model without cracks. The calibrated value of E for the diagonal brace reinforced model was greater compared to the ladder reinforced model. This might be due to the larger strut angle in the diagonal brace reinforcement model compared to the ladder reinforcement model. Nowak *et al.* [20] also reported that with the increase in the angle formed between the compressive strut developed in the model and the bed angle, there is an increase in the value of E.

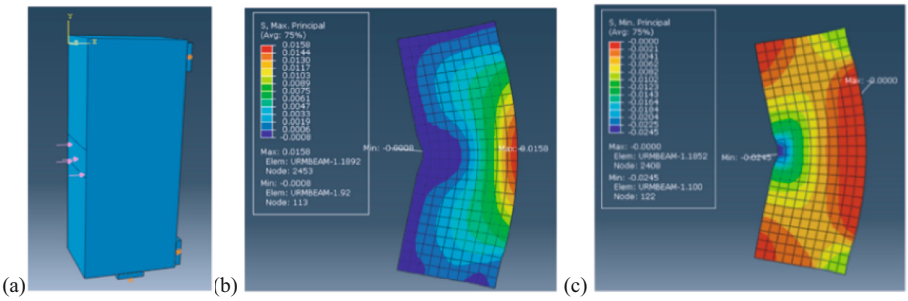

Fig. 7. (a) URM model (b) Tensile principal stress of URM model (c) Compressive principal stress of URM model

3.6 Effect of Elastic Modulus in Compression and Tension in URM Model

Kanno *et al*. (2001) reported that the elastic modulus in tension (E_t) for URM is in the range of 1/5–1/6 of that in compression (E_c) as E in tension and compression sides differ greatly. Therefore, in this study, E on the tension side of URM model was taken as 1/5 of E on the compression side. The tensile zone in the URM model in this study was chosen in such a way that the compressive strut formation still occurs between the supports and the loading point. By trial and error, the numerical result was in good agreement with the experimental value for maximum displacement (0.352 mm) at the mid-point for the T-shaped area on the tensile side with a lower value of elastic modulus (E_t = 1/5 of E_c) (Fig. 10a). Numerical result matched the experimental value when the E_c was 41 MPa and E_t was 8.2 MPa for URM model (Fig. 10a) (Table 6). Similarly, for the diagonal braced reinforced model with tensile crack, the numerical result showed the maximum displacement (1.615 mm) when E of 41 MPa was taken (Table 5). This might be due to the angle of the compressive strut formed with the bed angle (56.3°) being equal for both models [20].

Table 4. Numerical and experimental results of displacement at the mid-point of three models

Specimens	Load P (N)	E (MPa)	θ_{strut} (°)	Num. disp. (mm)	Exp. disp. (mm)
URM model	618	23.00	56.30	0.352	0.352
Ladder model	6520	16.45	37.20	3.533	3.533
Brace model	6520	38.00	56.30	1.615	1.615

Where, E is elastic modulus of brick masonry, θ_{strut} is the strut angle, Num. disp. is numerical displacement, and Exp. disp. is experimental displacement

Table 5. Numerical and experimental results assuming a crack in the tension side of masonry in reinforced model

Specimens	Load P (N)	E (MPa) with crack (70 mm)	E (MPa) with crack (90 mm)	E (MPa) with crack (130 mm)	θ_{strut} (°)	Num. disp. (mm)	Exp. disp. (mm)
Ladder model	6520	20.5	22.5	27.0	37.2	3.533	3.533
Brace model	6520	41.0	43.0	47.0	56.3	1.615	1.615

Where, E is the elastic modulus of brick masonry, θ_{strut} is strut angle, Num. disp. is numerical displacement, and Exp. disp. is experimental displacement

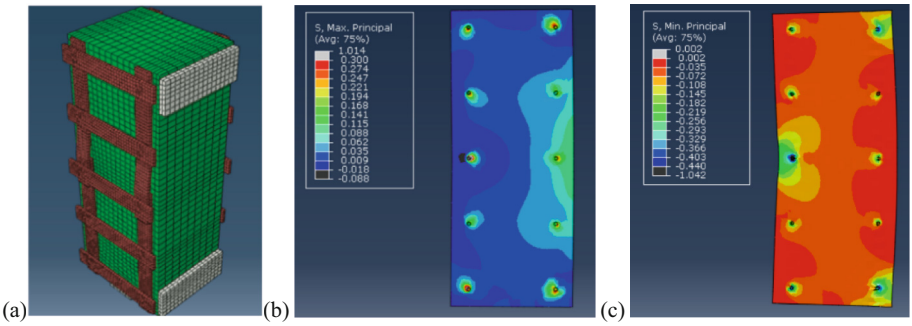

Fig. 8. (a) Ladder reinforced model (b) Tensile principal stress for ladder reinforced model (c) Compressive principal stress for ladder reinforced model

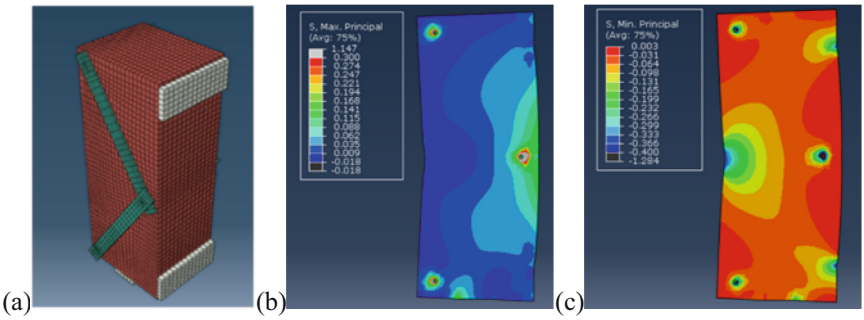

Fig. 9. (a) Diagonal brace reinforced model (b) Tensile principal stress for diagonal brace reinforced model (c) Compressive principal stress for diagonal brace reinforced model

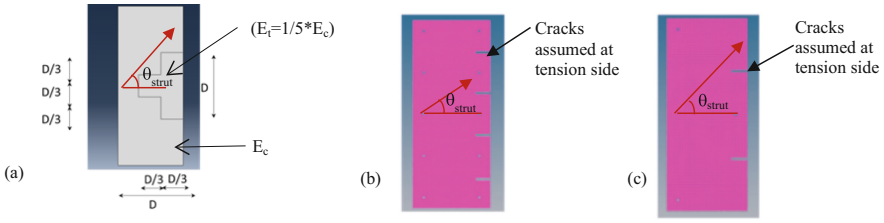

Fig. 10. Model for (a) URM specimen with different elastic modulus in compression and tension side (b) ladder reinforced specimen with cracks in the tension side of masonry (c) diagonal brace reinforced specimen with cracks in the tension side of masonry

Table 6. Numerical and experimental results of the URM model by considering $E_t = 1/5$ of E_c

Specimens	Load P (N)	Elastic modulus in Compression (E_c) (MPa)	Elastic modulus in Tension (E_t) (MPa)	θ_{strut} (°)	Num. disp. (mm)	Exp. disp. (mm)
URM model	618	41.0	8.20	56.3	0.352	0.352

Where, θ_{strut} is strut angle, Num. disp. is numerical displacement, and Exp. disp. is experimental displacement

4 Conclusions

1. A homogenous macro model was used to reproduce a previously performed three-point bending test of a prism built of brick masonry in earth mortar. In this study, the elastic modulus in tension (E_t) was considered 1/5 of that in compression (E_c) for unreinforced brick masonry (URM) prism.
2. Numerical model for the URM prism gave closer results to experimental value when E_c was 41 MPa which was 1/8 of E calculated from the uniaxial compression experiment (310 MPa).
3. In uniaxial compression test, the direction of compressive strut formed was 90° to the bed angle, and E determined was 310 MPa. However, in three-point bending test, compressive strut was formed from the point of loading to the supports. For URM and diagonal braced specimens, the compressive strut formed was 56.3° to the bed angle (θ_{strut}) whereas for ladder reinforced specimens, it was 37.2°.
4. For the ladder and diagonal braced reinforced model, crack was assumed at the tensile side of the masonry. By trial and error, the numerical result was in good agreement with the experimental value for maximum displacement at the mid-point under the condition that the E of 20.5 MPa and 41.0 MPa was taken for the ladder and diagonal brace model, respectively, with a 70 mm crack at the tensile side of masonry.
5. In the analysis, it was observed that for URM and diagonal brace reinforced model, E was greater compared to ladder reinforced model. Namely, with the increase in compressive strut angle (θ_{strut}), there was an increase in the value of E. This numerical result tends to coincide with the findings of Nowak et al. [20]

Acknowledgement. The experiment in this study was supported by JSPS KAKENHI Grant Number JP16H01825 and the analysis was supported by JSPS KAKENHI Grant Number JP22K04411.

References

1. Ravichandran, N., Losanno, D., Parisi, F.: Comparative assessment of finite element macro-modelling approaches for seismic analysis of non-engineered masonry constructions. Bull. Earthq. Eng. **19**(13), 5565–5607 (2021). https://doi.org/10.1007/s10518-021-01180-3

2. Varum, H., et al.: Structural behaviour and retrofitting of adobe masonry buildings. In: Costa, A., Guedes, J.M., Varum, H. (eds.) Structural Rehabilitation of Old Buildings, pp. 37–75 (2004)
3. Parisi, F., Iovinella, I., Balsamo, A., Augenti, N., Prota, A.: In-plane behaviour of tuff masonry strengthened with inorganic matrix–grid composites. Compos. B Eng. **45**(1), 1657–1666 (2013)
4. Arya, A.S., Boen, T., Ishiyama. Y.: Guidelines for Earthquake Resistant Non-Engineered Construction. UNESCO (2014)
5. Phaiju, S., Pradhan. P.M.: Experimental work for mechanical properties of brick and masonry panel (2018)
6. Endo, Y., Yamaguchi, K., Hanazato, T., Mishra, C.: Characterisation of mechanical behaviour of masonry composed of fired bricks and earthen mortar. Eng. Fail. Anal. **109**, 104280 (2020)
7. Shrestha, H. D., Subedi, J., Rajbhandari, M.: Seismic retrofitting guidelines of buildings in Nepal. Kathmandu, Nepal: Government of Nepal, Ministry of Urban Development, Department of Urban Development and Building Construction (2016)
8. Langenbach, R.: Bricks, mortar and earthquakes. APT Bull. **31**(3–4), 31–43 (1989)
9. Moreira, S., Ramos, L.F., Oliveira, D.V., Lourenço, P.B.: Experimental behavior of masonry wall-to-timber elements connections strengthened with injection anchors. Eng. Struct. **81**, 98–109 (2014)
10. Sustersic, I., Dujic, B.: Seismic strengthening of existing concrete and masonry buildings with crosslam timber panels. In: Materials and Joints in Timber Structures: Recent developments of Technology, pp. 713–723. Springer Netherlands (2014)
11. Maduh, U.J., Shedde, D., Ingham, J., Dizhur, D.: In-plane testing of URM Wall panels retrofitted using timber strong-backs In: Proceedings of the Australian Earthquake Engineering Society 2019 Conference, Newcastle, Australia, vol. 29 (2019)\
12. Dizhur, D.Y., Giaretton, M., Giongo, I., Ingham, J.M.: Seismic retrofit of masonry walls using timber strong-backs. SESOC J. **30**(2), 30–44 (2017)
13. Oliveira, L M.F.D.: Theoretical and experimental study of the behavior of vertical interfaces of interconnected structural masonry walls" (Doctoral dissertation, Universidade de São Paulo) (2014)
14. Dauda, J.A., Silva, L.C., Lourenço, P.B., Iuorio, O.: Out-of-plane loaded masonry walls retrofitted with oriented strand boards: numerical analysis and influencing parameters. Eng. Struct. **243**, 112683 (2021)
15. Parisi, F., Balestrieri, C., Varum, H.: Nonlinear finite element model for traditional adobe masonry. Constr. Build. Mater. **223**, 450–462 (2019)
16. Mishra, C., Yamaguchi, K., Endo, Y., Hanazato. T.: mechanical properties of components of nepalese historical masonry buildings (2018): In: Proceedings of International Exchange and Innovation Conference on Engineering and Sciences, vol. 4, No. 1, pp. 118–123
17. Kanno, T., Kino, J., Furuya. T.: Applicability of concrete structural analysis method to brick structure. In: 56th Annual Conference of the Japan Society of Civil Engineers (October 2001). vol. 110, pp. 220–221 (2 pages) (Japanese)
18. Mishra, C., Yamaguch, K., Araki, K., Ninakawa, T., Hanazato, T.: Structural behavior of brick wall specimens reinforced on the surface with RC walls under horizontal loading. J. Adv. Concr. Technol. **19**(6), 593–613 (2021)
19. Kim, S., Fujita, K., Hanazato. T.: Restoration of seismically-vulnerable historical masonry structures struck by an earthquake Part 3 Micro tremor measurement and damage of multi-storied pagodas by 2015 Nepal Gorkha earthquake. In: 2017 AIJ Conference 31–3 September (2017), Hiroshima, Japan (2 pages) (Japanese)
20. Nowak, R., et al.: Strength parameters of clay brick walls with various directions of force. Materials **14**(21), 6461 (2021)